Matthan: Drone Presence Detection by Identifying Physical Signatures in the Drone's RF Communication

Phuc Nguyen[†‡], Hoang Truong[†‡], Mahesh Ravindranathan[‡], Anh Nguyen[†‡],
Richard Han[‡] and Tam Vu[†‡]
[†]University of Colorado, Denver, [‡]University of Colorado, Boulder
{phuc.v.nguyen, hoang.truong,anh.t4.nguyen, tam.vu}@ucdenver.edu,
{mahesh.ravindranathan, richard.han}@colorado.edu

ABSTRACT

Drones are increasingly flying in sensitive airspace where their presence may cause harm, such as near airports, forest fires, large crowded events, secure buildings, and even jails. This problem is likely to expand given the rapid proliferation of drones for commerce, monitoring, recreation, and other applications. A cost-effective detection system is needed to warn of the presence of drones in such cases. In this paper, we explore the feasibility of inexpensive RF-based detection of the presence of drones. We examine whether physical characteristics of the drone, such as body vibration and body shifting, can be detected in the wireless signal transmitted by drones during communication. We consider whether the received drone signals are uniquely differentiated from other mobile wireless phenomena such as cars equipped with Wi-Fi or humans carrying a mobile phone. The sensitivity of detection at distances of hundreds of meters as well as the accuracy of the overall detection system are evaluated using software defined radio (SDR) implementation.

1. INTRODUCTION

With the advent of inexpensive commercially available unmanned aerial vehicles (UAV), drones are rapidly rising in popularity as a host of a wide class of applications ranging from commercial delivery [27], environment monitoring [2], photography [26], policing [81], fire fighting [73], just to name a few. However, with the rise in drone usage, there has also been a rise in incidents involving drones, such as mid-air collisions, damage to property, and violations of privacy.

In particular, drones are increasingly flying in sensitive airspace where their presence may cause harm, such as near airports, forest fires, large crowded events, and even jails. For example, Dubai airport, the third busiest airport in the world, reported that in 2016 it had to shut down three times to avoid unauthorized drone activity [16]. In 2015, drones were used to smuggle drugs and contraband into a Maryland prison [59]. A quadcopter crashed on the White House lawn [36], raising concerns about the safety of buildings and

political leaders. The presence of drones has interfered with and grounded aircraft fighting forest fires [46]. Drone crashes have also disrupted sporting events such as the US Open tennis tournament as well as a World Cup skiing race [79, 15]. In fact, based on FAA data, more than 300 drone incidents were reported in California alone between April 2014 and Jan 2016 [74], which is equivalent of 15 incidents per month on average or 1 incident every two days.

A variety of approaches have been explored to interdict drones. These include shooting nets at the drones to tamper with their propeller to bring them down [66], using lasers to shoot down drones [78], spoofing GPS to confuse a drone's localization system [33], hijacking the software of drones by hacking into them [58], using other drones to hunt down unauthorized drones [16], and even training eagles to attack and disable drones [4].

However, these interdiction strategies typically presume that the presence of the drone has already been detected. Recent work has sought to develop drone detection systems that leverage either microphone, camera, or radar to sense the presence of drones [23, 20, 1]. Each approach has its own limitations. Audio-based approaches can be confused by other sounds in noisy environments, has limited range, and cannot detect drones that employ noise canceling techniques [49]. Camera-based approaches require good lighting conditions, high quality lens, and camera with ultra-high resolution for detecting drones at long distance. Thermal and IR imaging cameras for long distance are prohibitively expensive and have limited coverage. Radio-frequency techniques based on active radar introduce RF interference. Geofencing is useful to prevent drones from flying into fixed areas known a priori as sensitive [74], but requires manufacturers to install such software and is less useful to prohibit drones from flying around temporary event venues (we refer readers to the related work Section 6 for thorough discussions of advantages and drawbacks of each approach).

In this paper, we consider an approach to detect the presence drone by passively eavesdropping on the RF communication between a drone and its controller (Wi-Fi standard). Such communication mode often happens over standard unlicensed spectrum for which a low-cost COTS hardware can be utilized for observation. Prior work utilizing passive RF to identify drones has sought, for example, to detect the frequency of transmission, the MAC address of the drone, and the frequency of packet communication [19, 57, 53]. All these techniques suffer from various limitations, as described in the related work section, and none seek to discern whether

physical signatures of the drone's motion are manifested in the drone's RF signal.

In this work, we investigate the fundamental aerodynamic and motion control mechanisms of drones to identify two key inherent types of movement of the drone's body, namely *body shifting* caused by the spinning propellers and *body vibration* due to navigation and environmental impact corrections. We validate our hypothesis on the existence of such movements through empirical studies and then conduct a theoretical analysis on the characteristics of such movements. We also explore the feasibility of reconstructing such movement by using passive RF sensing. We then propose Matthan, a system that incorporates a number of algorithms to detect the presence of drone from both body vibration and shifting. It employs low cost software-defined radios (SDRs) to eavesdrop on Wi-Fi channels used in drone-to-controller communication. We demonstrate that this system can detect the physical signatures to uniquely identify an individual drone and effectively differentiate it from other mobile wireless devices at distances of hundreds of meters. Matthan is currently able to detect Wi-Fi embedded individual drones independently at any point in time. We are investigating detection of drones that communicate at other RF frequencies to identify multiple drones at the same time.

Our paper makes the following contributions. We

- identify the relationship between the drone controller's compensation reaction and its body shifting

- identify a second frequency component in the RF signal that we attribute to the drone's propellers

- show that both of these on-board physical phenomena are manifested in the received RF signal

- devise an algorithm to detect drones from their RF-based signature based on both body vibration and body shifting physical characteristics marked on the continuous data stream between drones and their controllers

- verify that this algorithm can detect drone signatures at Wi-Fi frequencies that are uniquely differentiated from other mobile Wi-Fi devices, such as cars and walking cellphone users

- confirm that this algorithm can operate at distances of hundreds of meters using a directional antenna with a 21 degree beamwidth

- discover that this algorithm could be used to begin differentiating the seven different drones tested

In the following, we first describe in Section 2 the basics of drone flight and validate, using sensors attached to the drone, that the drone vibrates at the propeller frequency and that body shifting causes correlated disturbances in the RF signal. In Section 3, we develop a model to explain the influence of both types of body motion on the RF signal, and present our drone detection algorithm, which utilizes both frequency analysis to detect body vibration in the RF signal and wavelet analysis to detect shifts in the drone during flight. We provide a performance evaluation in Section 4 considering different types of evidence, then conduct an analysis over a variety of drones, environments, and distances. We conclude the paper with a discussion of the current drawbacks of Matthan, related work, and a summary.

2. FUNDAMENTAL AERODYNAMICS AND PHYSICAL SIGNATURES OF DRONES

Matthan relies on the unique physical signatures that persist across drones to detect and differentiate them from other moving objects. In this section, we start by providing the background on aerodynamic principles that allows drones to move towards a desired direction or remain balanced while flying. We then derive two unique physical signatures, namely *body shifting* and *body vibration*, that are present on all drones that have propellers. We empirically prove the existence of such signatures and then perform a formal analysis to show how such signature can be captured from the radio signals that are emitted from the drones for communicating with their remote controller.

2.1 Drone Movement and Control Background

Drones or micro air vehicles (MAVs) can be made from a form of helicopter, an airplane, a multirotors or even a balloon. In that, helicopter and multirotors are the most common drones due to simplicity of manufactoring. As its name indicated, a multirotor [43] has multiple rotors with a much simpler flying control mechanism compared to that of a helicopter [31]. Instead of changing its wing's pitch and speed using a complex rotor as found in helicopters to maintain balance and maneuver, a multirotor operates by simply changing its motors' speed. Therefore, no complex mechanical parts is required. Partly due to this simplicity, multirotor-based drones are much more popular than their counterpart helicopters [45]. Since it has multiple similar rotors arranged symmetrically, a multirotor can keep its balance more easily even when it carries additional load (e.g. cameras, packages). The change in the center of mass can be tolerated by simply adjusting the rotors' speed. These advantages of multirotor become even more significant when it comes to small-sized drones since integrating sophisticated controlling mechanics as in a helicopter requires a large form factor, increasing cost and size of the drone's footprint. Therefore, most of today's commercial drones are of the multirotor type and the same trend is predicted for the near future [63]. As a result, we focus on this type of drone in this paper.

Drone equilibrium conditions. The popular designs of multirotors include 4-, 6-,and 8-rotors which are naturally termed quadcopter, hexacopter and octocopter respectively. The most popular one is the quadrotor, which has four similar propellers arranged in either "×" configuration or "+" configuration with equal distance from its the center of mass. The rotation direction of each propellers depends on its relative position. Let the indexes of the propellers be numbered sequentially from #1 to #4. If the propeller #1 rotates clockwise, for example, the ones #2 and #4 will rotate counter-clockwise while #3 will rotate clockwise as illustrated in Figure 1. To facilitate our analysis in the remaining sections of this paper, let ω_i with $i = 1..n$ be the rotation speed of each propeller. Without losing the generality, we only focus on analyzing quadrotors ($n = 4$).

Let F_i with $i = 1..4$ be the forces generated by the propellers i and m be the mass of the quadrotors. Since the quadrotor is symmetric, if L is the distance between the center of the quadrotor and each propeller, the moment generated by each propeller is calculated by $M_i = L * F_i$. In an ideal environment, in order to keep balance and remain
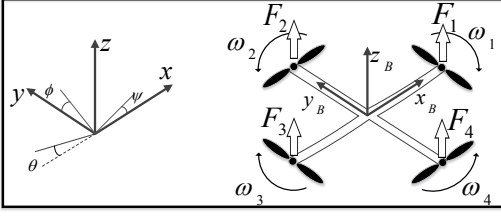
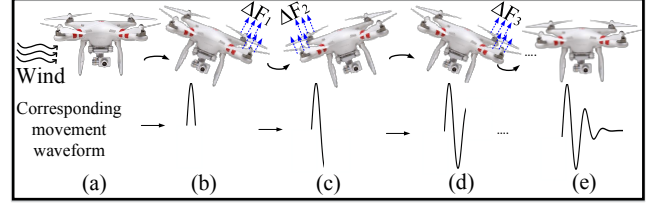Figure 1: Earth and quadrotor reference systems.

Figure 2: An example illustrated the drone shifts its body due to the effect from an unexpected wind. The additional force ΔF are created by speeding up corresponding propellers to balance the drone.

in equilibrium state, the quadrotor must obey these four physical conditions:

(1) $\sum_{i=1}^{4} F_i = -mg$ (Equilibrium of forces),
(2) $\sum_{i=1}^{4} F_i \| g$ (Equilibrium of directions),
(3) $\sum_{i=1}^{4} M_i = 0$ (Equilibrium of moments), and
(4) $(\omega_1 + \omega_2) - (\omega_3 + \omega_4) = 0$ (Equilibrium of rotation speeds).

If one or more of those conditions are violated, the quadrotor will leave equilibrium state and start making movement as depicted in Figure 1. Two reference systems are used to represent the position and orientation of the quadrotor. The inertial reference system, i.e. the Earth frame (denoted x, y, z-axes) provides the absolute linear position of the quadrotor; and the quadrotor reference system, i.e. the Body frame (denoted x_B, y_B, z_B-axes) gives the angular position with three Euler angles. Roll angle (ϕ), Pitch angle (θ) and Yaw angle (ψ) determine the rotation of the quadrotor around the x, y, z-axes respectively.

Drone maneuvering conditions. Any movement of a quadrotor can be created by a combination of four basic movements: roll rotation, pitch rotation, yaw rotation and altitude change. Each of these movements is created by briefly violating the above equilibrium conditions by applying proper angular speeds to each propeller, $\omega_{1..4}$. For example, to create a roll rotation, $\omega_{1..4}$ must be applied such that $(\omega_1 + \omega_4) - (\omega_2 + \omega_3) \neq 0$. Similarly, to generate a pitch rotation, the drone needs to change the angular speeds of different rotors such that $(\omega_1 + \omega_2) - (\omega_3 + \omega_4) \neq 0$. To move the drone up and down, the rotation speeds should be changed to adjust the thrust force F so that $\sum_{n=1}^{4} F_i \neq -mg$.

2.2 Body Shifting and Body Vibration as Drone's Physical Signatures

Many different controllers have been introduced in the literature following aforementioned principles, including PID [72, 21, 83, 8], back-stepping [41, 82], nonlinear H∞ [62], LQR [8], and nonlinear controllers with nested saturation[12, 24], to stabilize and maneuver drones. Beside taking the desired direction as inputs, these controllers also need to take into account the impacts of the unpredictable environments, such as wind, and the inaccuracy of its sensors and actuators. Since these factors are nondeterministic and occur often, the controller needs to frequently react to and compensate for them, causing undesirable physical movement of the drone. In particular, the undesirable movements can be the result of the controller's reaction to (a) an environmental change, e.g., a gust of wind, a magnetic storm; (b) numerical errors inside control loop of the drone itself, e.g. the imperfection of converting from speed of rotation to the exact targeted pitch, roll, yaw angles [31, 32, 9]; and (c) by the vibration caused by propeller's movement [31]. We leverage these undesirable yet persistent movements as unique signa-

tures of drones, which can be used to differentiate a drone from other moving objects. The movements of interest fall into two main categories: *the drone's body shifting* and *the drone's body vibration.*

Drone body shifting. Body shifting occurs as a sequence of discrete events. Figure 2 illustrates the drone's body movement caused by wind (a, b) as the result of a rebalancing effort from the drone's controlling mechanism (c, d). Beside the drifting its body does due to the effect of environmental conditions, the drone body also usually changes its body orientation and direction when it flies. The angular velocity of the rotor i, denoted ω_i, creates force F_i in the direction of the rotor's axis. The angular velocity and acceleration of the rotor also need to create torque τ_{M_i} around the rotor axis: $F_i = k\omega_i^2, \tau_{M_i} = b\omega_i^2 + I_M\omega_i^*$ in which ω_i is the rotation speed of rotor i, k is the lift constant, b is the drag constant, the inertial movement of the rotor is I_M. The impact from ω_i^* is usually small and thus it is omitted. When the wind creates an additional force that changes the balance of the drone, the drag force now becomes $\tau_{M_i} + \Delta F_1$. To make the drone return to a stable state, the propeller on the right side will speed up to create an additional force $\Delta F_2, (\Delta F_1 \approx \Delta F_2)$ against the force generated by the wind. When the drone is balanced, if the additional force ΔF_2 stays longer than expected, it creates a side effect to the drone body that makes the drone unbalanced again. Next, the controlling algorithm will changes the propeller speed expecting the drone to go to the balanced state. This process will be repeated and take several iterations until the drone gets to its equilibrium. We consider this behavior to be one signature of a flying drone that can be used to distinguish it from other flying objects, e.g. birds. Because of the waveform's resemblance to a wavelet, this stimulated our interest in developing a wavelet-based detector for drone body shifting, as explained later.

Drone body vibrations. The drone body is vibrated within a certain frequency range and such vibrations are usually caused by the rotation of its propellers [31, 32]. In the literature, several works have been conducted to analyze the vibration of helicopters caused by their propeller's rotation [38, 30, 40]. The resulting vibration is the vector sum of vertical, longitudinal, and lateral vibrations. More specifically, in forced vibration, the frequency of the vibration is close to the frequency of the force or motion applied, and the magnitude of the vibration depends on the actual mechanical system [5]. The steady-state solution of the forced vibration system with damping subjected to a sinusoidal force $F(t) = F\sin(2\pi ft)$ can be expressed as $x(t) = X\sin(2\pi ft + \phi)$, where $x(t)$ is the vibration func-

tion, X is the amplitude of the vibration, f is the vibration frequency, which is the same as the engine operating speed, and ϕ is the phase.

Thus far, we have discussed two types of drone's inherent body movements that happen when the drone is flying. However, these types of movement are unexplored in the literature. To validate our hypothesis, we conduct a set of experiment to validate the drone body shifting and body vibration signatures. We also conduct a feasibility check to confirm whether an RF-based technique can be used to detect the drone by observing its signatures.

2.3 Preliminary Validation of Drone Body Movements

This section presents a set of experiments to validate the signatures of the drone as mentioned earlier. We conduct two main experiments to explore the body movement characteristics of the drone using (1) inertial measurement units (IMUs) and (2) a wireless sensing hardware. In the first experiment, we attach external IMUs, to the drone's frame underneath each propeller to capture the drone's body movements. Secondly, we also attach firmly a 2.4 GHz wireless transmitting antenna to the drone. The RF signal from the transmitter is captured by a wireless receiver placed 2 meters apart. The goal here is to validate whether the drone body movements are observable by analyzing the received wireless samples. We present results here from experiments conducted for the Parrot Bebop [56] in an indoor environment. Similar confirmation was obtained using the DJI Phantom [22].

2.3.1 Validating Drone Body Movements using IMUs

We inspected behaviors of the drone including taking off, hovering, and flying. The drone is augmented with 4 IMUs (MPU 9150 [69]) each of which is mounted beneath propeller. The data from these IMUs are gathered by an Arduino Pro Mini board [3] and then are sent to a computer via Bluetooth Module HC-05 [7]. A camera was also used to record the start, the end, and the movement of the drone during testing sessions. The objectives of the experiments are to answer the following questions: *(a) Does the drone vibrate and move its body when flying as predicted in the previous analysis?, (b) What are the frequencies of such vibrations and movement patterns?, (c) When there is no wind, will the drone body shifting still persist?*

The spectrogram of the collected signal is shown in Figure 3. There are two dominant frequencies that are observable from the data. The low frequency (less than 10Hz) components happen at 10^{th}(s), 20^{th}(s), 32^{th}(s), 40^{th}(s), and 53^{th}(s), which correspond to the drone's body shifting (confirmed from recorded videos). In addition, the second dominant frequency at 50th to 70th Hz represents the vibration frequency of the drone body caused by propellers. These results answer the first two questions we mentioned earlier, that the drone constantly vibrates and create iterative body shiftings when it flies. The observed data also shown that the body vibration and body shifting can happen at the same time at some moments.

To answer the third question, we setup a closed indoor experiment where wind is blocked to a minimal level and the drone circles within a small room. Analyzing the captured IMU data in both time and frequency domain gives us two conclusions: the drone body vibration is still present from
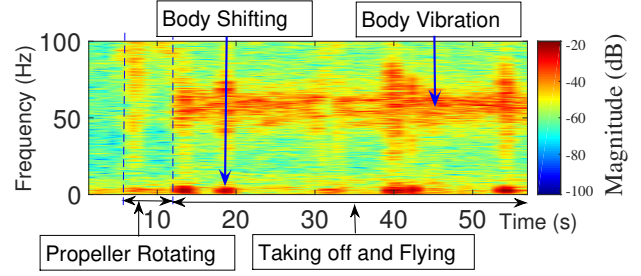

Figure 3: An example illustrates the movement captured by IMUs attached to the Bebop drone.

the IMU data even without wind; and the body shifting still happens during the time the drone tries to adjust its pitch and yaw angles to fly in a circular shape. Such drone body movements happen when the drone tries to change its pitch, roll, and yaw angles. In summary, we empirically confirmed that the drone body is shifted even in a windless environment, and the drone body continuously vibrates when it flies. In the next subsection, we will conduct another experiment to validate whether those movements can be captured using RF signals.

2.3.2 Feasibility Check: Capturing Drone Body Movements using RF Signals

We conduct the second set of experiments to check the feasibility of capturing the drone movements using RF signals. A wireless transmission antenna is attached to the drone. A wireless receiving antenna is placed at a fixed location to capture the signal sent from the transmitter (which is attached to the drone as illustrated in Figure 4). We used USRP B200 mini software-defined radios (SDR) [77] to control the transmitter and receiver antennas. The antennas are connected to USRP SDRs through cables of 6m length. The transmitter antenna emits a single tone wireless signal at 2.4 GHz when the drone is flying. The key idea is to capture the change in RSSI and phase of the transmitted single tone signal to infer the drone body movements. In addition, we also attached the IMUs to the drone and collect the data as the ground truth. The objectives of this experiment are to answer the following questions: *Do received wireless samples correspond to the movements of the drone (a) for body shifting? and (b) for body vibration?*
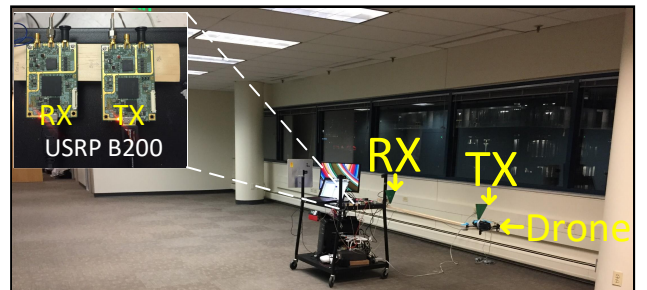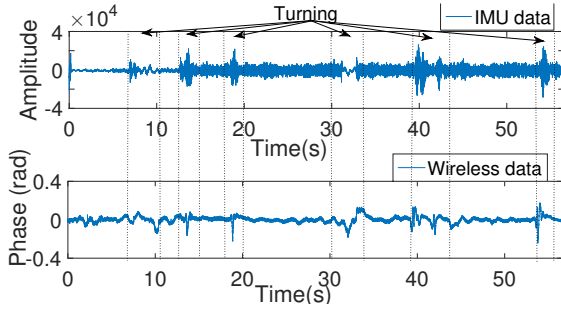

Figure 4: The setup for the indoor environment.

The results showed that it is possible to capture body shifting and body vibration in the RF domain. First, in Figure 5, we plot the raw data obtained from accelerometer

Figure 5: Signals captured by the IMU and from RF.

data and the phase of the received RF signal. Note that the SDR listens to a WiFi band and demodulates the signal to baseband, after which we compute the FFT. As shown in the figure, the body shifting peaks corresponding to turning are clearly identifiable and correlated on both accelerometer and RF data.
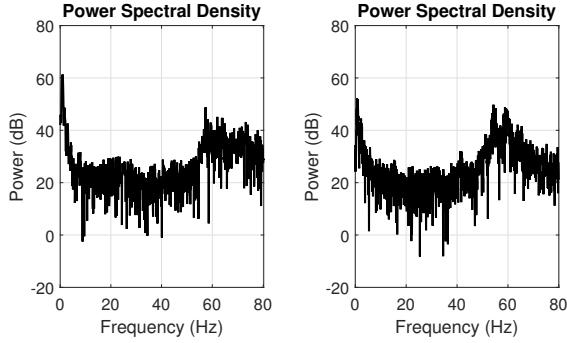
Figure 6: The frequency distribution of the signal from IMU (left) and RF (right).

We conducted experiments to see whether the measured vibration frequency of the IMU matches what we see in the frequency domain of the RF signal. We confirmed that the peak frequency detected in the frequency domain repeatedly matches what we observed via the IMUs. Figure 6 illustrates the frequency distribution of RF signal captured with peaks around the 60 Hz mark, which is similar to the peak on the IMU measurements.

3. MATTHAN DRONE PRESENCE DETECTION

We design Matthan, a system that detects the above-mentioned body movements, namely body shifting and body vibration, by passively listening on the radio channels that the drone is using to communicate with its remote controller. A number of algorithms are introduced to capture such miniature physical signatures and to identify if it is coming from a drone. In the following subsection, we first formally define our problem and identify challenges in realizing such a system. We then present the body vibration detection method and body shifting detection method before describing a fusion algorithm that combines the two types of movements into a single classifier.

3.1 Problem Formulation

To detect the presence of drones, Matthan listens to the channel that is used by the drones to communicate with its remote controller. Let the signal broadcast by the drone to its remote control be $\tilde{t}(t)$ at time t. The signal Matthan received by listening is $\tilde{r}(t)$. Since the movements of interest are at frequencies that are a few orders of magnitude lower than the carrier frequency or the data rate, $\tilde{r}(t)$ can be filtered to obtain only the low frequency components. Let $\tilde{r_f}(t)$ be the filtered signal. We then have:

$$\tilde{r_f}(t) = q(t) + \eta(t) \qquad (1)$$

where $q(t)$ is the signal that contains the drone body shifting and body vibration, and $\eta(t)$, which is the environment noise. After removing the DC components, $\eta(t)$ becomes a signal with zero-mean and some variance. Previous experiments show that the drone body vibration happens continuously over a specific range of frequencies when the drone is flying. In addition, we also found that the drone body shifting has a form that is close to a wavelet $\psi(t)$ due to the characteristic of its rebalancing and control loop mechanisms. Hence, the drone signal $q(t)$ can be written as:

$$q(t) = \psi(t) + X sin(2\pi ft + \phi) \qquad (2)$$

where $\psi(t)$ is the function represents the drone body shifting. $\psi(t)$ is the function containing different dominant single tone cosine signals that have amplitude $\hat{A}(\psi)$, frequency $\hat{f}(\psi)$, and phase $\hat{\phi}(\psi)$. And X, ϕ, and f are the amplitude, phase, and frequency of the drone body vibration. In summary, the key objectives of Matthan are to identify the drone body shifting $(\hat{A}(\psi), \hat{f}(\psi), \hat{\phi}(\psi))$ and the drone body vibration (X, ϕ, f).

■ **Challenges.** However, accurate and robust drone detection based on RF signals is hard due to the following challenges:

1) Movements-RF translation. The drone body shifting and movement information are buried in the wireless signal. This limits the maximum detection range that can be obtained from the system at different environment.

2) The body shifting can happen at different scales. Different drones creates different types of body shifting according to their controlling mechanism and accuracy as well as their physical characteristics (weight, structures, and etc.). The signal can be detected at different magnitudes as well as frequencies. However, the shape of the body shifting signal stays relatively constant. We propose a wavelet based technique that is resilient to the scale and magnitude of the physical body shift.

3) Interference from static APs. The drone may communicate at the same frequency channel with the wireless APs in the environment. The detection algorithm should be able to distinguish between the signals from the static APs and the signal from the drone. The solution for the next challenge is used to solve this problem.

4) Interference from mobile APs. A mobile AP carried by a human walking or an embedded AP on a moving vehicle, e.g. bus, could create similar wireless signals as the drone, which could affect the detection results (assuming the AP operates at the same frequency with the drone's communication channel). We propose a technique that differentiates the drone from other static or mobile APs based on identifying the body vibration of the drone using RF.

5) Environment noise. The noisy and heterogeneous environment makes the problem much more challenging. We introduce an evidence-based classifier to make the detection more robust. The drone presence is detected based on the availability of multiple lines of evidence that uniquely identify the physical characteristics of the drone (i.e., body shifting and body vibration).

6) Variety of drones. Drones vary in terms of having different numbers of propellors, weights, sizes, speeds, and communication mechanisms. We present a confusion matrix showing that Matthan's detection approach is promising in terms of discriminating among the specific set of drones that we tested.

3.2 Drone Detection Algorithm

In this section, we present Matthan's detection algorithms. Since the drone body shifting happens at different scales and environments, it can be detected at different magnitudes as well as frequencies. However, the shape of the signal stays relatively constant. We propose a wavelet-based technique that is resilient to the scale and magnitude of the physical body shift. In addition, we design a Fourier analysis to detect the drone body vibration. We then design an evidence-based algorithm taking the input from wavelet and Fourier analysis to make the final decision.

3.2.1 Drone Body Shifting Detection

We use wavelet analysis to detect the drone body shifting. A wavelet is a wave-like oscillation with an amplitude that begins at zero, increases, and then decreases back to zero. Wavelets are especially good at capturing brief oscillations. From the results of our experiment (Sec. 2.2), the behavior of the drone body shifting is similar to the form of a wavelet. This characteristic will result in high coefficients when multiplying the wireless signal $\tilde{r}(t)$ with scaled versions of the mother wavelet.

The wavelet, denoted by $w(t)$, maintains local information in both the time and frequency domains. It is defined as a waveform that satisfies the following condition: $\int_{-\infty}^{+\infty} w(t)dt = 0$. The Wavelet Transform [71] uses as the wavelet that satisfies the condition of dynamic scaling and shifting function, $w_{s,p}$,

$$w_{s,p}(t) = \frac{1}{\sqrt{s}}w\left(\frac{t-p}{s}\right) \qquad (3)$$

where $w_{s,p}(t)$ are the integrated and integral transformation signal, s is the scale and p is the shift parameter, which can also be the central location of the wavelet in the time domain. The wavelet can be stretched and translated with flexible windows by adjusting s and p, respectively. The wavelet transform of the wireless received samples $\tilde{r}(t)$ using transform coefficient $W(s,p)$ is calculated as following:

$$\begin{aligned} W(s,p) &= \int_{-\infty}^{+\infty} \tilde{r_f}(t)\overline{w_{s,p}}(t)dt \\ &= \frac{1}{\sqrt{s}}\int_{-\infty}^{+\infty} \tilde{r_f}(t)\overline{w_{s,p}}\left(\frac{t-p}{s}\right)dt \end{aligned} \qquad (4)$$

where $\overline{w_{s,p}}(t)$ represents the complex conjugate of $w_{s,p}(t)$. The result of the wavelet transform gives us a correlation function of the template signal at different scales (frequency bands) in both the time and frequency domains. As in Equation 4, the correlation function $W(s,p)(t)$ has two main fea-
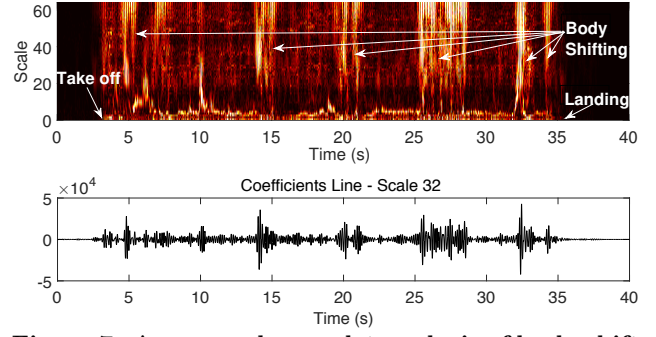
Figure 7: An example wavelet analysis of body shifting detection

tures as follows. (1) The time resolution is high with high frequencies while the frequency resolution is high with low frequency signals. When multiplying the high frequency component of the signal with the high frequency of the wavelet, the correlation result will indicate the exact location where it happens. This can be used to identify the very first body shifting event created by the drone. (2) As the wavelet has local existence in both time and frequency domain, the point of discontinuity in the signal can be detected with high sensitivity. As the discontinuity (generated by body shifting) is considered as an event and happens quickly in time, the result of correlation with high frequency wavelet will be readily captured.

Let $W_m(s,p)$, $W_{vi}(s,p)$, and $W_\eta(s,p)$ be the wavelet transform coefficients of the signal caused by the drone body shifting, drone body vibration, and the noise, respectively. The wavelet transform coefficient of the sum of the signals is calculated as follows:

$$W_{m+vi+\eta}(s,p) = W_m(s,p) + W_{vi}(s,p) + W_\eta(s,p) \qquad (5)$$

Because of the linearity property, the coefficients of the wavelet transform enable us to precisely identify the body shifting event in the time domain when there is a signal discontinuity. As the drone body vibration and the noise are quite constant over time, these behaviors decay quickly after different levels of scaling, leaving the body shifting component. The wavelet transform coefficients then give us two valuable pieces of information for event detection: the location and the duration of each body shifting event. Figure 7 (top) depicts the results of the wavelet transform at 64 scales of the received wireless samples where the drone body shifting events are correctly identified.

To identify exact time and frequency of the drone body shifting, Matthan decomposes the signal into a sequence of sub-frequency bands and approximates the energy of each frequency band. Energy of each sub-frequency is calculated as following:

$$\xi_i = \int |f_i(t)|^2 dt = \sum_{k=1}^{n} |f_i(k)|^2 \qquad (6)$$

where $f_i(t)$ is the signal of i frequency band, $f_i(k)$ is its discrete value. The system compares the energy of each frequency band, then reconstructs the coefficient of special sub frequencies that have enough energy and contain the frequency of drone body shifting.

The center of the signal can be calculated according to the definition of the gravitational center in mechanics, namely

the center of the body shifting event in time is given as:

$$t_{center} = \frac{\int t|f(t)|^2 dt}{\int |f(t)|^2 dt} \qquad (7)$$

Then, the width of the window function of the STFT can be calculated from the central point to the point where the coefficient value $W_{s,p}$ drops down to the noise band. Hence, the above results gives us the time center and the width of the function. We then can perform STFT to analyze the frequency of the drone body movement. The peak of the frequency distribution resulting from STFT identifies the frequency of drone body shifting $\psi(t)$.

3.2.2 Drone Body Vibration Detection

As seen earlier in Figure 3, the drone's vibration creates a periodic signal that is well-reflected in the FFT-based spectrogram. Conversely, a wavelet transform that is better-suited for capturing transitory phenomena such as a body shifting event is not well-suited for drone vibration detection. Consequently, we employ a frequency domain approach to identifying the presence of the drone's vibration signal. Recall that the wireless signal component that is affected by the drone body vibration has the form of $Xsin(2\pi ft + \phi)$. From the received wireless sample $\tilde{r}(t)$, an efficient approximation of the drone's vibration frequency is to identify the dominant frequency component that has maximum power spectrum density (PSD) through the STFT. Then, the approximation of the drone's vibration frequency f_v is as follows:

$$f_v = \max_{[f_{min} \to f_{max}]} \left(|\sum_{k=1}^{N} \tilde{r}_f(t)e^{-j2\pi ftk}|^2 \right) \qquad (8)$$

where N is the number samples. After f is estimated, it can be used to estimate the amplitudes and phases of different frequency channels using the following: $X = \frac{2}{N} |\sum_{k=1}^{N} \tilde{r}_f(t)e^{-j2\pi ftk}|$, and $\phi = actan\frac{-\sum_{k=1}^{N} \tilde{r}_f(t)sin(2\pi ftk)}{\sum_{k=1}^{N} \tilde{r}_f(t)cos(2\pi ftk)}$. In this way, the system obtains the desired quantities $[X, \phi, f]$.

3.2.3 Evidence-Based Drone Detection Algorithm

We design an algorithm to determine if a drone is present by first gathering evidence from multiple sources that relate to drone body shifting and vibration, then combine these sources of evidence to form a binary classifier. The overview structure of Matthan is illustrated in Figure 8.
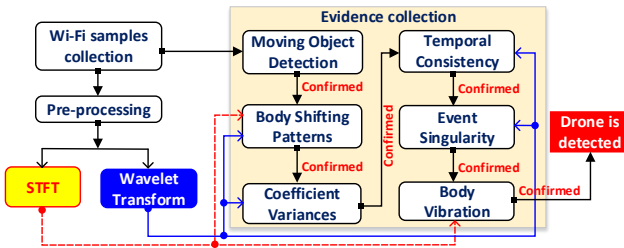

Figure 8: Overview architecture of Matthan.

■ **Evidence #1: Moving Object**. The first evidence to collect is the presence of a moving object using RF signals. This of course is not a unique indication of a drone but of

any moving object such as a human walking while carrying a phone or a phone inside a car. Matthan calculates the standard deviation of the received wireless signal and compares it with the standard deviation of the environment at the time of initialization. The standar deviation of the signal without moving objects, denoted by δ_0 is an environment independent quantity [76] and it represents the received signal changes caused by electronic noise. Received signals are dominated by *quantization errors* and *electronic noise*. Therefore, the signal follows a Gaussian distribution with zero-mean after DC removal [76]. On the other hand, when the drone or other moving object is in the environment, the received signals are expected to follow the distribution of multipath fading because it dominates the other noise sources. A log-normal, Ricean, or Rayleigh distribution is expected to represent the distribution of the collected data with such multipath affects. As a result, the comparison between the standard deviation of the signal at test and δ_0 can be done to confirm this evidence.

■ **Evidence #2: Drone Body Shifting**. As mentioned in Section 3.2.1, the drone body shifting event serves as one of the main indications of drone presence detection. Since the shifting follows a certain pattern in space, it can be amplified and detected using wavelet transformation. We use Mexican hat wavelet [67] as the template of comparison because this wavelet has a similar waveform to the drone's body shifting event shown before. It is important to note that the speed (i.e how fast it shifts) and amplitude (i.e. how much it moves) of the shifting might vary from one movement to another. Therefore, our evidence confirmation method must be designed to detect a specific range of speeds (i.e. frequency) and amplitudes (i.e. wavelet scale). We propose a two-step process for confirming the body shifting by looking at the signal from both frequency and wavelet domains. In particular, we (1) acquire the frequency of the body shifting as shown in Section 3.2.1. We then (2) compare the waveform of the shifting with the template by calculating the coefficient between the two using the Dynamic Time Wrapping technique [28, 75]. The evidence is confirmed when the frequency is less than 5Hz and the coefficient is under a preset threshold. This threshold is determined by the practical possible range of body shifting amplitude.

■ **Evidence #3: Coefficient Invariance**: This evidence is to confirm that the body shifting is a discrete event that is similar to the template. The intuition for this evidence stems from the fact that body shifting movements are unexpected and non-uniform events triggered by various environmental and electronic artifacts. As a result, two or more consecutive body shifting motions are not expected to be similar. As one of the wavelet transformation properties, coefficient invariance can be used to confirm if a template is present on a trunk of signal once and only once. In particular, the coefficients are retained and even enhanced as the transformation scale increases [13] for each body shifting event. Hence, if the signal is of the template form and non-repetitive for 4 consecutive body shifting cycles, the body shifting event is confirmed. In short, the coefficient invariance evidence is confirmed if the coefficient magnitude monotonically increases across multiple body shifting events detected by evidence #2 as the transformation scale increases.

■ **Evidence #4: Temporal Consistency**: While the previous evidence (#3) can capture the discontinuity and repetitive of an event, it could also introduce false positive by counting *short* and *discrete surges* of signals caused by noises in the environment. This evidence is introduced to address this very issue. The key idea is to observe the spread of the signal at different sampling rates. As the sampling rate reduces, the coefficient of the noise (discrete surges) decays because the wireless samples that represent the surges are reduced or disappear. Let t_1 be the spread of the signal at sampling rate f_{s1}, t_2 be the spread of the signal at sampling rate f_{s2}, $f_1 > f_2$. t_1 and t_2 can be approximated from the spread of the wavelet coefficient that is over the threshold. Wavelet decomposition [44] is used to collect this evidence. If t_1 and t_2 at two consecutive levels of decomposition are close to each other, the evidence is confirmed.

■ **Evidence #5: Event Singularity**: As the fluctuation of the drone is in the wavelet pattern, the direction of fluctuation is very unique. The direction of the body shifting can be obtained by the sign of extremum of the *wavelet coefficients*. The direction must be changed between two consecutive extrema at the same frequency with that of the body shifting at different levels of decomposition. To confirm the fluctuation is from the drone body, the sign of the extremum coefficient needs to alternate while the magnitudes of coefficients remain similar. While evidence #2 shows the similarity of the signal representing body shifting and the template, evidences #3 and #4 make sure there is no false positive due to the noises in the RF domain, evidence #5 confirms that the change of body shifting behavior should cross-interleave the balance state.

■ **Evidence #6: Drone Body Vibration**: As shown in subsection 3.2.2, the drone body vibration is observable through a short-time Fourier analysis. The evidence is obtained when maximum power distribution of the peak frequency belongs to the range of drone's body vibration. This evidence is used to identify the drone versus other interference sources such as mobile AP carrying by a walking user or the embedded AP on a moving vehicle.

The different forms of evidence are collected at each time window. The decision is made based on the number of forms of evidence that are confirmed on each window. We sort the evidence based on their uniqueness as the signature for drones. All the evidence is combined linearly for the final decision of detection. That is, Matthan concludes a drone is present only when all the forms of evidence are confirmed. In Section 4, we show the contribution of each form of evidence to the accuracy of Matthan.

4. PERFORMANCE EVALUATION

4.1 Experimental Setup

We implement Matthan using the SDR USRP B200 mini [77]. The USRP board is sampled at 100kHz to collect wireless samples from the drone's communication channel. The USRP board is configured as a receiver connecting to a 2.4GHz 20dBi gain directional antenna [37]. The wireless samples collected from USRP are sent to a laptop for data processing and filtering. The Wi-Fi channel of the drone's communication is identified by Wi-Fi Analyzer [25]. This application provides the channel ID and frequency for listening to the drone's communication. The collected data are stored in binary files and further processed using MATLAB.

We conducted experiments in three different environments including a parking lot in the downtown of a city (*urban*), a soccer field inside our university (*campus*), and an open field (*sub-urban*) as depicted in Figure 9. In each environment, the data are collected when the drone is flying at different distances with respect to our receiver. We collect data at the maximum distance of 100m, 200m, and 600m in urban, campus, and sub-urban environments, respectively. The drone is controlled to *take off* and *hover* within the coverage area of the antenna receiver's beam during all experiments.
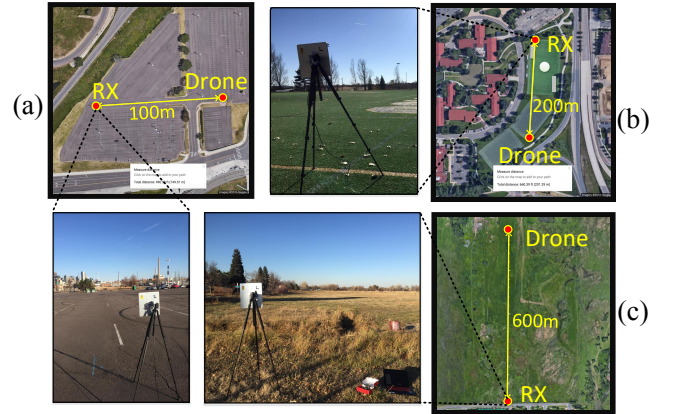
Figure 9: Testing locations: (a) Urban (Parking area), (b) University campus, and (c) Sub-urban

The experiment was conducted on 7 different drones of different models and manufacturers as shown in Figure 10, including the Parrot Bebop [56], Protocol Dronium One Special Edition [60], Sky Viper [68], Swift Stream [70], Parrot AR DRone [55], Protocol Galileo Stealth [61], and DJI Phantom [22]. The Bebop, Dronium, Skype Viper, ARDrone, and DJI Phantom send Wi-Fi signals from the Wi-Fi card mounted on their body for either controlling the channel or streaming video. Protocol Galileo Stealth and Swift Stream emit Wi-Fi signals from the plug-n-play cameras came with the drones.
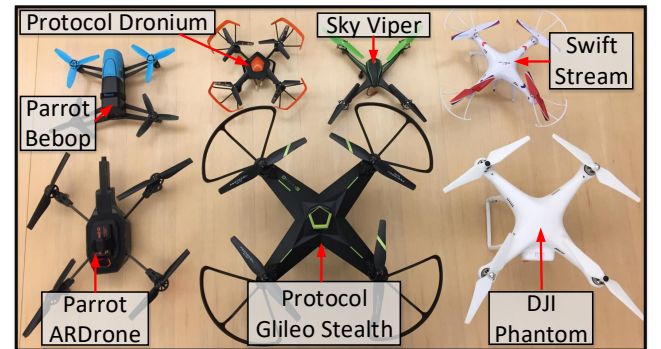
Figure 10: Drones used during experiments

To test whether the drone's RF signal could be differentiated from those of other mobile wireless devices, we also
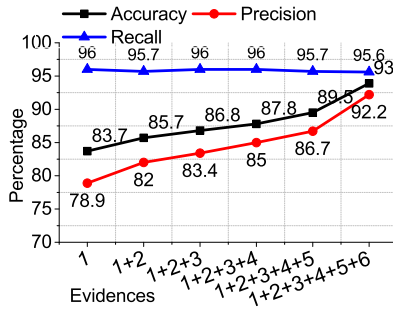
Figure 11: Detection accuracy with increasing forms of evidence.

Figure 12: Detection accuracy at different distances.

Figure 13: Detection accuracy at long distances.

evaluated two other scenarios when a mobile AP was carried inside a moving vehicle or by a walking person. First, the user configures a mobile device to create a Hotspot (mobile AP) to emit Wi-Fi signals. We use another mobile phone (client phone) to connect to the mobile AP. The client phone streams Youtube video continuously. We asked the user to carry both client and the mobile AP to walk around at a distance of 50m away from the wireless system. Secondly, the client and mobile AP are placed inside a car which moves around in the coverage area of the wireless system at a distance of 50m to 100m away. The vehicle is moving at 20 mph (32 km/h) speed. In both scenarios, the mobile AP and client are always within the coverage area of the system.

We then segmented the collected data into two main types: *drone* and *no drone*. Each segment has a length of 10 seconds. The "drone" data contains the wireless segments that correspond to the moment where the drone is flying in the environment. Similarly, the "no drone" data contains the wireless segments that correspond to the moment at which there is no drone in the environment (the drone is completely turned off). More specifically, the "no drone" data contains types of data including "environment noises", "human carrying mobile AP", and "mobile AP augmented inside a car".

4.2 Evaluation Results

In this section, we evaluate the performance of Matthan at different distances (from 10m to 600m), with 7 different types of drones, and at different environmental setups (urban, campus, sub-urban). We use *accuracy*, *precision* and *recall* as the performance metrics for evaluation. The *accuracy*, *precision*, and *recall* are calculated from True Positive (TP), True Negative (TN), False Positive (FP), and False Negative (FN). The calculations are given as follows: $accuracy = \frac{TP+TN}{TP+FP+FN+TN}$, $precision = \frac{TP}{TP+FP}$, and $recall = \frac{TP}{TP+FN}$.

4.2.1 Detection Performance vs. Number of Evidences

As stated in Section 3, Matthan makes detection decision by collecting evidences that are resulted from its analysis of the collected wireless samples.

We run the evaluation on the segmented data set of 600 segments of 10 seconds data (300 segments of drone's presence and 300 other segments from the environment, human walker carrying mobile AP, and mobile AP inside a moving car). This data is collected when the Bebop is at 50m distance from the Matthan system. The performance of detection is shown in Figure 11 in which the evidence IDs are corresponding to the IDs presented in Section 3. As can be
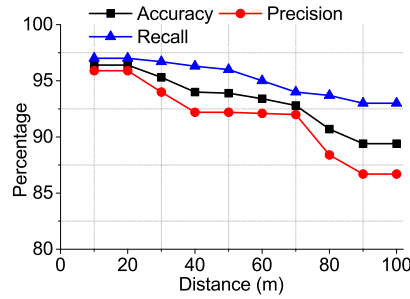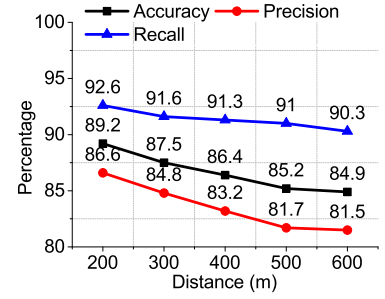
seen, the accuracy of the system is as low as 83.7% when the system uses only the first form of evidence to detect the drone. More importantly, the system obtained a precision of detection around 78.9%. Such performance is not really usable for reliable detection. So, the first evidence only helps to detect the drone in an environment where the system receives minimal interference from other Wi-Fi sources. However, based on this evidence, Matthan cannot detect the drone within environments that contain a large amount of interference. When more evidences are combined, the performance increases significantly. More specifically, we can observe how the false positive rate diminishes and precision correspondingly rises as more evidences are integrated. Initially, the precision of the system is as low as 78.9% with only one part of evidence and increases successively to 86.7% once the first five forms of evidence are considered. Matthan does not recognize all of the wireless samples representing a human carrying an AP or a mobile AP inside a car as drone data because the standard deviations of the wireless samples in these cases are sometime smaller than the detection threshold. From our observations, the standard deviations of the signal in these scenarios are only incorrectly identified as the signal from the drone only when the user goes toward or backward Matthan (with distance less than 5m). Finally, when the vibration detection is considered (evidence #6), the overall *precision* rises to 92.2% (corresponding with 93.9% of *accuracy* and 95.6% for *recall*). This result is obtained due to the fact that the last evidence is well-represented for the uniqueness of drone's body vibration in the environment.

4.2.2 Impact of distance

We also analyze the impact of the distance between the detection system and the drone on Matthan's performance. The evaluation is conducted for both short and long distances. At short distances, we analyze the performance of the system when the drone is from 10m to 100m away. Bebop data from the urban environment experiment is presented for this analysis. At each location, 600 segments of data are analyzed (300 segments of drone's presence). All 6 forms of evidence are used to calculate the results of detection. The results are shown in Figure 12. The system obtained up to 96.5% of *accuracy*, 95.9% of *precision* and 97% of *recall* when the drone is 10m away from the detection system. When the distance increases, the performance of the detection falls to 89.4% of *accuracy*, 86.7% of *precision* and 93% of *recall* at 100m. Note that with audio-based detection techniques, the most recent report shows that the
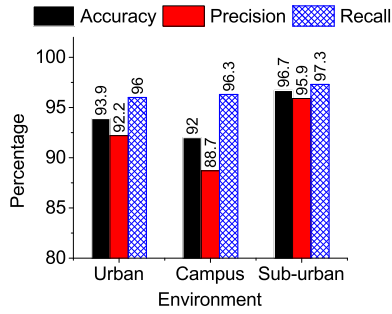
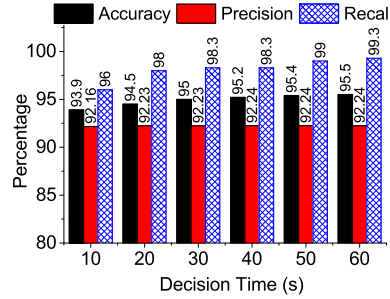Figure 14: Detection accuracy in different environments.

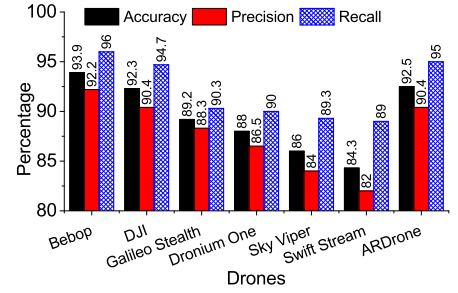Figure 15: Detection accuracy with different decision times.

Figure 16: Performance across different drones.

drones are correctly detected with distance less than 30m, and this technique completely fails with distance more than 50m [29]. Similarly, video techniques can be performed for detection at distances less than 50m with large drones [65, 64].

The Matthan's performance is further evaluated when the distance between the drone and Matthan is from 200m to 600m. We used a sub-urban data set for this evaluation. We used 200 segments (100 segments with drones' presence) at each distance to evaluate the system. Figure 13 shows the performance of Matthan at these longer distances. The system obtained 84.9% of *accuracy*, 81.5% of *precision*, and 90.3% of *recall* at 600m distance. We were limited to 600m due to the space constraints of the testing location, but hope to find another venue with greater range.

4.2.3 Impact of environmental setup

We also evaluate the impact of the environment noise to Matthan's performance. We use the 50m data set from the Bebop drone at three locations (urban, campus, and sub-urban) for this evaluation. The impact of mobile APs is also taken into account. One half of the data set are from the drone, another half includes the data from the environmental noises and human carrying a mobile AP. The data from mobile APs inside the campus environment is not available because we cannot drive a car inside the campus. The results of drone detection are shown in Figure 14. We use 600 segments of data and 300 segments from the drone's presence. The system obtained the best performance in the sub-urban environment as this area has little effect from environmental noise as well as multi-path reflection. The system can achieve up to 96.7% of *accuracy*, 95.9% and 97.3% of *precision* and *recall*, respectively. The campus environment has a number of wireless access points operating over different Wi-Fi channels, and hence it is found that the drone communication channel usually interferes with other static APs in the campus environment. At the time of the experiment, there were 16 Wi-Fi APs in the same vicinity using Wi-Fi Analyzer app [25]. Therefore, the system creates more false alarms (false positive) in the campus environment compared with urban and sub-urban environments. However, Matthan still performs 92% of *accuracy*, 88.7% of *precision* and 96.3% of *recall* in the most interfering environment (campus).

4.2.4 Impact of time budget

Detecting the drone is also challenging due to the limited time budget within which the drone flies across the detection system. We are interested in analyzing the detection accuracy of Matthan with different time budgets for detection. The key motivation is to understand the performance when the drone stays longer inside the coverage area. We use the data set from the Bebop drone at 50m distance in an urban environment for this evaluation. We use 600 segments of data with 300 segments from the drone's presence. We increase the duration of each measurement (segment) from 10s to 60s, and a decision is made for each segment. Figure 15 shows the performance obtained for different time budgets. Matthan obtains up to 95.5% of accuracy with 60s budget of detection. The *accuracy* and *recall* increase as we give more time for Matthan to make a decision, unlike the *precision*.

4.2.5 Performance across different drones

We evaluate the performance of Matthan for different types of drones including Parrot Bebop [56], Protocol Dronium One Special Edition [60], Sky Viper [68], Swift Stream [70], Parrot AR DRone [55], Protocol Galileo Stealth [61], and DJI Phantom [22]. Galileo Stealth and Swift Stream and some small drones in the market are usually configured at a specific frequency that does not belong to any Wi-Fi's channel. These drones are very light-weight and cannot carry much weight. They usually utilize a Wi-Fi camera for video streaming and navigation. As the camera is attached to the drone, the wireless signal emitted by the Wi-Fi camera would be very similar to the controlling signal from the drones if there is no shock absorbing mechanism is in-place for the camera. We found that it is the case in the drone of our procession in this experiment. Figure 16 shows the accuracy of detecting different drones using Matthan. Matthan performs with the highest detection results for heavy drones such as Bebop, DJI, Galileo Stealth, and ARDrone. We found that those four drones generate similar signatures in body shifting as well as vibration frequency range. The Dronium and Swift Stream drones are more light-weight. We observed that there was less vibration generated in the light-weight drones than the heavier ones, which explains the improved results for the heavier drones.

4.2.6 Drone classification

It is also important to identify which drone is flying in the coverage area after detecting its presence. Though it is not the focus of this work, we want to explore if it is even possible with Matthan. We conducted a classifier based on the physical characteristics of the drones to detect them. The key idea is to identify the frequency of vibration of each drone to detect/classify it. Drones are often uniquely designed in weight, structure, materials, propellers' size and so on. .

Drone	Bebop	DJI	Galieo	Dronium
f_v (Hz)	60	100	140	35
Drone	**Sky Viper**	**Swift Stream**	**AR Drone**	
f_v (Hz)	50	20	70	

Table 1: A table summary of the vibration frequency of different drones f_v.

Those characteristics affect the forces generated by the propellers and therefore also affect the vibration frequency of the drones. We employed a similar experimental setup as in section 2.3.1. We attached the IMUs to different drones to collect the motion data. The motion data is then analyzed to determine the central and the dominant frequencies of vibration. According to this central frequency, we approximate the vibration frequency windows as in Table 1.
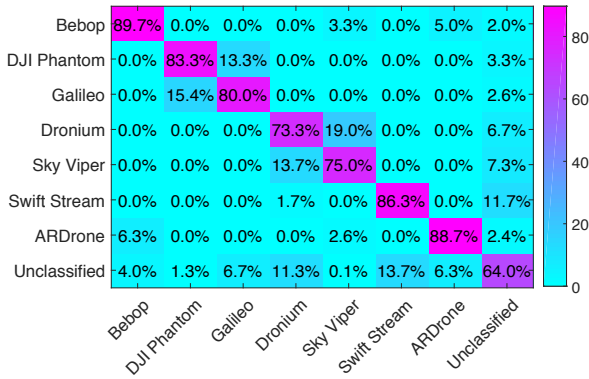
Figure 17: Confusion matrix from drone classification based on FFT analysis.

5. DISCUSSION

Our system has focused on detecting the presence of drones through their unique inherent physical movement signatures on WiFi domain. We wish to expand our experiments to consider a wider variety of drones and greater distances. Our system should be expanded to incorporate automated channel sensing [47, 48, 14, 35], as the current experiments fix the eavesdropping to a specific communication channel. Such an approach should improve our ability to detect diverse drones that operate with different protocols over the same unlicensed Wi-Fi frequency bands, or that communicate on non-Wi-Fi frequency bands. Our system should also be enhanced to integrate automated antenna steering/ beamforming, as our current experiments fix the direction of the antenna. Note that the directional antenna is only used for improving the gain of detection at a certain direction, omi-directional antenna can also be used to detect the presence of the drone. Localizing the position of the drones is the next logical step, but this consideration is outside the scope of this paper.

We would like to conduct experiments that test non-line-of-sight RF detection in the presence of occlusions such as buildings. We intend to pursue further the extent to which Matthan can distinguish between individual drones as well as different types of drones. We also desire to conduct a more detailed examination of fusion algorithms such as boosting and bagging for combining multiple weak detectors into a stronger fused detector. In addition, we wish to detect other

aspects of the drone beyond merely its presence, such as its location, speed and direction. Also in the future we hope to address the fact that our system is not currently capable of detecting multiple drones in the same vicinity at the same time. Moreover, we would like to evaluate the impact of the environment, e.g. windy condition, to the accuracy of detection. Finally, while reactive control [9] is considered as one solutions to reduce a number of body-shifting events, Matthan's algorithm can be slightly modified to update the weight of each evidence to focus more on the impact of the drone's body vibration in detection.

6. RELATED WORK

Multiple sensing modalities have been employed for drone detection, including audio, video and RF. First, an acoustic approach collects a database of acoustic signatures from different drones and uses this database to compare with observed sound signals to make a decision [23]. Challenges to this approach include detection accuracy in noisy urban environments and at distance, keeping this database updated, and new quieter drone models [50].

Second, a video-based solution employs a camera to detect drones [20]. Challenges to this approach include operation at night, compute-intensive image processing that must distinguish between a drone and say a bird at distance, and occlusion by buildings that limit distance in an urban environment. Thermal cameras have been proposed to detect drones at night [34] but are a relatively expensive technique.

A variety of RF-based solutions have been proposed for drone detection. One approach is to monitor the 1MHz - 6.8GHz band, and any unknown transmitter is assumed to be a drone [19]. This would suffer from false positives. Another approach is MAC address collection and analysis [57], but this can be bypassed easily by spoofing the MAC address. The frequency of packet communication on the uplink and downlink between the drone and its controller has also been used for detection[53]. However, other periodic packet sources at similar rates such as VOIP traffic could be mistaken as drone communication.

Radar-based techniques actively transmit RF waves and look for the reflection to determine the presence of the drone. WiDop [1] is a non-coherent radar system which exploits the modulation produced by a target in a clutter with a non-coherent X-band radar. WiDop is claimed to have advantages over a coherent radar in terms of low cost radar and high range, but there exist disadvantages due to the radar angle and lack of high precision. Another radar technique is passive bistatic radar [80, 10, 52, 51, 54], which consists of a passive receiver to process a received signal from a known source of transmission and reflected signals from the moving target. These systems have advantages of low cost, fast update of the target position and variable frequency allocation. In conjunction with the usage of abundant WiFi sources as reference transmitters, multiple algorithms [17, 6] have been proposed for signal processing in passive bistatic radar systems such as MTI and LS adaptive filters [11] or compressive sensing [42]. Moreover, multistatic radar [18, 39], which includes more than two receivers, is also used to detect flying objects by calculating the radar cross section. The use of multiple receivers increase the accuracy of the system. Radar generally introduces interference due to active transmissions, which is especially problematic when there is a large amount of legitimate packet traffic over RF bands such as Wi-Fi, especially in crowded environments.

7. CONCLUSION

This paper introduced Matthan, a system for detecting the presence of drones by identifying unique signatures of a drone's body vibration and body shifting in the Wi-Fi signal transmitted by a drone. The joint detector integrates evidence from both a frequency-based detector that looks for the maximum frequency peak to be in the range of 50-220 Hz to indicate drone body vibration as well as a wavelet-based detector that captures the sudden shifts of the drone's body by computing wavelets at different scales from the temporal RF signal. Matthan was prototyped and evaluated using SDR radios in three different real-world environments. When given a mix of data containing both drone and non-drone cases (Wi-Fi-equipped car, walking user with a smartphone on, and no drone scenarios), we showed that Matthan is capable of differentiating drone signals from other mobile wireless devices by achieving high accuracy, precision and recall, all above 90 percent at 50 meters. We also showed how Matthan's accuracy, precision and recall varies with distance, dropping to 90 percent accuracy and 80-85 percent precision and recall at a distance of 600 meters. Matthan's performance was studied across seven different drones, where the performance varied only moderately, and was tested across three different environments, again varying only moderately in performance. We also present how Matthan's performance improves as it is allowed more time to accumulate data. Finally, a confusion matrix illustrates Matthan's potential to identify specific drones from among seven different drones.

Acknowledgements

8. REFERENCES

[1] R. Abileah, P. A. Fox, and J. W. Maresca Jr. Detection of low observable objects in clutter using non-coherent radars, Feb. 23 2016. US Patent 9,268,008.

[2] Amazon. Amazon prime air. https://goo.gl/Ags0YJ, 2016. [Online; accessed Nov 01, 2016].

[3] Arduino. Pro mini. https://goo.gl/AGFeCN, 2016. [Online; accessed Nov 01, 2016].

[4] BBC. Dutch police fight drones with eagles. https://goo.gl/PnJCcd, September 12, 2016.

[5] L. L. Beranek. Noise and vibration control engineering: principles and applications. Wiley, 1992.

[6] Berger et al. Signal processing for passive radar using ofdm waveforms. IEEE Journal of Selected Topics in Signal Processing, pages 226–238, 2010.

[7] Bluetooth. Bluetooth hc-05. https://goo.gl/0PKs6r, 2016. [Online; accessed Nov 01, 2016].

[8] S. Bouabdallah, A. Noth, and R. Siegwart. PID vs LQ control techniques applied to an indoor micro quadrotor. pages 2451–2456, 2004.

[9] E. Bregu, N. Casamassima, D. Cantoni, L. Mottola, and K. Whitehouse. Reactive control of autonomous drones. In ACM MobiSys, pages 207–219, 2016.

[10] J. Brown, K. Woodbridge, A. Stove, and S. Watts. Air target detection using airborne passive bistatic radar. Electronics letters, pages 1396–1397, 2010.

[11] Buonanno et al. Wifi-based passive bistatic radar by using moving target indicator and least square adaptive filtering. In IEEE International Symposium on Phased Array Systems & Technology, pages 174–179, 2013.

[12] Castillo et al. Real-time stabilization and tracking of a four-rotor mini rotorcraft. IEEE Transactions on Control Systems Technology, pages 510–516, 2004.

[13] P. Chaovalit et al. Discrete Wavelet Transform-based Time Series Analysis and Mining. ACM Comput. Surv., pages 6:1–6:37, 2011.

[14] R. I. C. Chiang et al. A Quantitative Analysis of Spectral Occupancy Measurements for Cognitive Radio. In IEEE VTC, pages 3016–3020, 2007.

[15] CNN. Drone crashes onto piste, misses champion skier by inches. https://goo.gl/jtPdLh, 2015. [Online; accessed Nov 01, 2016].

[16] CNN. Dubai deploys a 'drone hunter' to keep its airport open. https://goo.gl/iXJMu3, 2016. [Online; accessed Nov 01, 2016].

[17] F. Colone et al. A multistage processing algorithm for disturbance removal and target detection in passive bistatic radar. IEEE Transactions on Aerospace and Electronic Systems, pages 698–722, 2009.

[18] E. Conte et al. Multistatic radar detection: synthesis and comparison of optimum and suboptimum receivers. Communications, Radar and Signal Processing, IEE Proceedings F, pages 484–494, 1983.

[19] DDC-LLC. Domestic drone countermeasures. https://goo.gl/ZAju6O.

[20] DeDrone. Drone tracker. http://www.dedrone.com/en/, 2016. [Online; accessed Nov 01, 2016].

[21] I. C. Dikmen, A. Arisoy, and H. Temeltas. Attitude control of a quadrotor. In RAST, pages 722–727, 2009.

[22] DJI. DJI Phantom. http://www.dji.com/, 2016. [Online; accessed Nov 01, 2016].

[23] DroneShield. Drone detection. https://goo.gl/y5ZuMm, 2016. [Online; accessed Nov 01, 2016].

[24] J. Escareno, S. Salazar-Cruz, and R. Lozano. Embedded control of a four-rotor UAV. In American Control Conference, page 6, 2006.

[25] Farproc. Wifi analyzer. http://tinyurl.com/8yqxge9.

[26] J. Fleureau et al. Generic Drone Control Platform for Autonomous Capture of Cinema Scenes. In ACM MobiSys Dronet, pages 35–40, 2016.

[27] FlexReport. The economics of drone delivery. https://goo.gl/RN4irU, 2016. [Online; accessed Nov 01, 2016].

[28] T. Giorgino. Computing and visualizing dynamic time warping alignments in R: The dtw package. Journal of Statistical Software, pages 1–24, 2009.

[29] L. Hauzenberger and E. H. Ohlsson. Drone detection using audio analysis. Master's thesis, Department of Electrical and Information Technology, Lund University, Lund, Scania, Sweden, 2015. https://goo.gl/58BGoN.

[30] R. Heffernan et al. Vibration analysis of the SA349/2 helicopter. NASA Technical Memorandum 102794, 1991.

[31] G. Hoffmann et al. Quadrotor Helicopter Flight Dynamics and Control: Theory and Experiment. In *AIAA Guidance, Navigation and Control Conference and Exhibit*. 2007.

[32] H. Huang et al. Aerodynamics and control of autonomous quadrotor helicopters in aggressive maneuvering. In *IEEE ICRA*, pages 3277–3282, 2009.

[33] T. HUMPHREYS. Statement on the security threat posed by unmanned aerial systems and possible countermeasures, 2015.

[34] IEC. IEC infrared systems: Banshee. https://goo.gl/TLDjFb, 2016. [Online; accessed Nov 01, 2016].

[35] M. H. Islam et al. Spectrum Survey in Singapore: Occupancy Measurements and Analyses. In *EAI CROWNCOM*, pages 1–7, 2008.

[36] B. Jansen. Drone crash at white house reveals security risks. USA Today, January 26, 2015.

[37] L-Com. 2.4 / 5.1-5.8 GHz 20dBi Flat Panel Antenna. https://goo.gl/77WdQD, 2016. [Online; accessed Nov 01, 2016].

[38] Y.-C. Lai and S.-S. Jan. Attitude estimation based on fusion of gyroscopes and single antenna GPS for small UAVs under the influence of vibration. *GPS Solutions*, pages 67–77, 2011.

[39] S. K. Laleh et al. Detection, identification and tracking of flying objects in three dimensions using multistatic radars. *Int'l J. of Communications, Network and System Sciences*, 2009.

[40] X. Liu and R. Randall. Blind source separation of internal combustion engine piston slap from other measured vibration signals. *Mechanical Systems and Signal Processing*, pages 1196–1208, 2005.

[41] T. Madani and A. Benallegue. Backstepping Control for a Quadrotor Helicopter. In *IEEE/RSJ IROS*, pages 3255–3260, 2006.

[42] P. Maechler et al. Compressive sensing for wifi-based passive bistatic radar. In *EUSIPCO*, pages 1444–1448, 2012.

[43] R. Mahony, V. Kumar, and P. Corke. Multirotor aerial vehicles: Modeling, estimation, and control of quadrotor. *IEEE robotics & automation magazine*, pages 20–32, 2012.

[44] S. G. Mallat. A Theory for Multiresolution Signal Decomposition: The Wavelet Representation. *IEEE Trans. Pattern Anal. Mach. Intell.*, pages 674–693, July 1989.

[45] Marketsandmarkets. Multirotor uav market worth $2.28 billion by 2020. https://goo.gl/1M43OD, 2016. [Online; accessed Nov 01, 2016].

[46] P. McGreevy. Private drones are putting firefighters in 'immediate danger,' california fire official says. LA Times, August 18, 2015.

[47] M. A. McHenry and S. Chunduri. Nsf spectrum occupancy measurement project summary. *Shared Spectrum Company Report*, 2005.

[48] M. A. McHenry et al. C. s. chicago spectrum occupancy measurements and analysis and a long-term studies proposal. *TAPAS*, 2005.

[49] Z. Naboulsi. Drone detection: What works and what doesn't. https://goo.gl/MkfHoF, 2016. [Online; accessed Nov 01, 2016].

[50] Newshub. Big noise for kiwis' quiet drone. https://goo.gl/ioa6hj, April 25, 2016.

[51] Nguyen et al. WiKiSpiro: Non-contact Respiration Volume Monitoring During Sleep. pages 27–29, New York, NY, USA, 2016.

[52] P. Nguyen et al. Continuous and fine-grained breathing volume monitoring from afar using wireless signals. In *IEEE INFOCOM 2016*, pages 1–9, 2016.

[53] P. Nguyen, M. Ravindranatha, A. Nguyen, R. Han, and T. Vu. Investigating cost-effective rf-based detection of drones. In *ACM MobiSys Dronet*, pages 17–22, 2016.

[54] N. P. et al. Continuous and Fine-grained Respiration Volume Monitoring Using Continuous Wave Radar. In *ACM MobiCom*, pages 266–268. ACM, 2015.

[55] Parrot. ARDrone. https://goo.gl/deJFd6, 2016. [Online; accessed Nov 01, 2016].

[56] Parrot. Parrot Bebop Drone. https://goo.gl/xZ36IF, 2016. [Online; accessed Nov 01, 2016].

[57] M. Peacock and M. N. Johnstone. Towards detection and control of civilian unmanned aerial vehicles. 2013.

[58] J.-S. Pleban et al. Hacking and securing the ar. drone 2.0 quadcopter: investigations for improving the security of a toy. In *SPIE Electronic Imaging*, 2014.

[59] W. Post. Prisons try to stop drones from delivering drugs, porn and cellphones to inmates. https://goo.gl/6DapQM, October 13, 2016.

[60] Protocol New York. Dronium ONE - Special Edition WiFi. https://goo.gl/u4NjuS, 2016. [Online; accessed Nov 01, 2016].

[61] Protocol New York. Protocol Galileo Stealth. https://goo.gl/TVGPkx, 2016. [Online; accessed Nov 01, 2016].

[62] G. V. Raffo and dothers. An Integral Predictive/Nonlinear H∞ Control Structure for a Quadrotor Helicopter. *Automatica*, pages 29–39, 2010.

[63] Reportbuyer. Global multi-rotor drone market - analysis and forecast 2016-2022 (focus on major applications payloads and, pricing). https://goo.gl/Z6Z2gF, 2017. [Online; accessed Apr 17, 2017].

[64] A. Rozantsev, V. Lepetit, and P. Fua. Flying Objects Detection from a Single Moving Camera. In *Conference on Computer Vision and Pattern Recognition (CVPR)*, 2015.

[65] A. Rozantsev, V. Lepetit, and P. Fua. Detecting Flying Objects using a Single Moving Camera. *IEEE Transactions on Pattern Analysis and Machine Intelligence*, pages 879 – 892, 2017.

[66] D. Sathyamoorthy. A review of security threats of unmanned aerial vehicles and mitigation steps.

[67] L.-K. Shark and C. Yu. Design of Matched Wavelets Based on Generalized Mexican-hat Function. *Signal Process.*, pages 1451–1469, 2006.

[68] Skyrocket. Sky Viper. http://sky-viper.com/, 2016. [Online; accessed Nov 01, 2016].

[69] Sparkfun-InvenSense. Mpu 9150. https://goo.gl/Hh3viK, 2016. [Online; accessed Nov 01, 2016].

[70] S. Stream. Swiftstreamrc. https://goo.gl/sB0Kro, 2016. [Online; accessed Nov 01, 2016].

[71] C. Taswell and K. C. McGill. Algorithm 735: Wavelet transform algorithms for finite-duration discrete-time signals. *ACM Trans. Math. Softw.*, pages 398–412, 1994.

[72] A. Tayebi and S. McGilvray. Attitude stabilization of a four-rotor aerial robot. In *IEEE CDC*, pages 1216–1221, 2004.

[73] Techcrunch. Firefighting drone serves as a reminder to be careful with crowdfunding campaigns. https://goo.gl/WwFgWk, 2016. [Online; accessed Nov 01, 2016].

[74] L. Times. To keep drones out of high-risk areas, companies try hijacking them and shooting them down. https://goo.gl/MqDag5, 2016. [Online; accessed Nov 01, 2016].

[75] P. Tormene et al. Matching incomplete time series with dynamic time warping: An algorithm and an application to post-stroke rehabilitation. *Artificial Intelligence in Medicine*, pages 11–34, 2008.

[76] D. Tse and P. Viswanath. *Fundamentals of Wireless Communication*. 2005.

[77] USRP. B200 Mini. https://goo.gl/7ssQDP, 2016. [Online; accessed Nov 01, 2016].

[78] R. Vander Schaaf. *What technologies or integrating concepts are needed for the US military to counter future missile threats looking out to 2040?* PhD thesis, US Army, 2014.

[79] D. Waldstein. Drone crash interrupts match. New York Times, September 3, 2015.

[80] N. J. Willis and H. D. Griffiths. *Advances in bistatic radar*. SciTech Publishing, 2007.

[81] Wired. Surrey now has the uk's 'largest' police drone project. https://goo.gl/VzrdQf, 2016. [Online; accessed Nov 01, 2016].

[82] K. M. Zemalache, L. Beji, and H. Marref. Control of an under-actuated system: application a four rotors rotorcraft. In *IEEEROBIO*, pages 404–409, 2005.

[83] Z. Zuo. Trajectory tracking control design with command-filtered compensation for a quadrotor. *IET Control Theory Applications*, pages 2343–2355, 2010.